Geochemical characteristics of basalts related to incipient oceanization: The example from the Alpine-Tethys OCTs

Méderic Amann, Marc Ulrich, Gianreto Manatschal, Eric Pelt, Marie-eva Epin, Julia Autin, Daniel Sauter

1   Geochemical characteristics of basalts related to incipient oceanisation: the example from the

2   Alpine-Tethys OCTs

3   Amann M.*[1], Ulrich M.[1], Manatschal G.[1], Pelt E.,[2] Epin M-E.[1], Autin J.[1], and Sauter D.[1]

4

5   [1]Institut de Physique du Globe de Strasbourg (IPGS)-EOST, CNRS-UMR 7516, Université de Strasbourg, 5, rue

6   René Descartes, 67084 Strasbourg, France

7   [2]Laboratoire d'Hydrologie et de Géochimie de Strasbourg (LHyGeS), CNRS-UMR 7517, Université de

8   Strasbourg, 1, rue Blessig, 67084 Strasbourg, France

9

Abstract

11   Basalts exposed in the Platta and Tasna nappes (SE Switzerland) derive from the Alpine-Tethys Ocean-

12   Continent Transitions (OCT) and overlie SubContinental Lithospheric Mantle (SCLM). We show that the trace

13   element signatures of these basalts differ from Mid-Ocean Ridge Basalts (MORB). Two types of basalts occur

14   in the OCT: a type-1 showing a "garnet signature" that can be modeled by the partial melting of the SCLM in

15   the spinel stability field and a type-2 characterized by an enrichment in incompatible elements that can be

16   explained by the mixing between garnet-pyroxenite-derived melts and the melting of either a depleted MORB

17   mantle or a refertilized SCLM. Based on geological and geochemical observations we propose that the basalts

18   from the Alpine-Tethys OCTs result from a poly-phase magmatic system that carry an inherited SCLM signature.

19   These basalts should therefore be referred to as OCT-basalts rather than as MOR-basalts.

20   *Keywords: Ocean-Continent Transition, Alpine-Tethys, basalt, inheritance, subcontinental mantle, OCT-*

21   *basalt.*

1. Introduction

The geochemical composition of mid-ocean ridge basalts (MORB) is due to the partial melting of a depleted mantle source (DMM). One remaining key question is whether basalts from magma-poor ocean-continent transitions (OCTs) are formed by similar melting processes as MORB or if they reflect more complex mantle processes associated with lithospheric thinning of a sub-continental lithospheric mantle (SCLM). Basaltic samples derived from present-day magma-poor OCTs are rare and limited to few samples drilled at the Iberia-Newfoundland (Chazot et al., 2005; Cornen et al., 1999; Robertson, 2007), the South China Sea (Sun et al., 2016) or the Diamantine OCT (Beslier et al., 2004; Chatin et al., 1998). In contrast, Alpine-Apennine ophiolites expose remnants of the OCTs of the ancient magma-poor Jurassic Alpine Tethys, which provide information not only on the basalts but also on the underlying mantle (Picazo et al., 2016). Previous studies on basalts derived from the fossil Alpine-Tethys OCT show that they are characterized by a wide range of trace element compositions, from depleted basalts (Bill et al., 2000; Desmurs et al., 2002; Durand-Delga et al., 1997; Kramer et al., 2003; Montanini et al., 2008; Piccardo, 2008; Saccani et al., 2008) to enriched basalts (Frisch et al., 1994; Renna et al., 2018; Steinmann and Stille, 1999; Vannucci et al., 1993) leading to various interpretations concerning the parental sources of these basalts. Over the last decade, a considerable data set has been acquired on the mantle rocks from Alpine-Tethys OCTs (Müntener et al., 2010; Picazo et al., 2016; Piccardo, 2016; Rampone et al., 2008). This new knowledge, combined with the geological observations, enable to better discriminate between the various interpretations and to understand the processes involved in magma-production at deeper parts of the lithosphere during mantle exhumation and lithospheric breakup.

In this paper, we present a compilation of Alpine-Tethys basalt chemistry including new data from the Platta and Tasna nappes (SE Switzerland, Fig. 1a). The lack of a major Alpine metamorphic overprint, the excellent exposure and the understanding of the mantle evolution prior and during breakup of these two nappes allowed to propose a tectono-magmatic model that may explain the peculiar geochemistry of the basalts of the Alpine-Tethys OCT.

2. Geological setting

2.1. Remnants of OCTs in the Alps

The Tasna and Platta nappes represent well preserved remnants of a fossil OCT of the ancient European and Adriatic conjugate rifted margins (Manatschal et al., 2006; Manatschal and Nievergelt, 1997) that were related to the opening of the Jurassic Liguro-Piemonte/Alpine Tethys ocean (Fig. 1b). This ocean probably was a narrow basin (<600km-wide) that developed as a result of an ultra-slow spreading activity (Marroni and Pandolfi, 2007; Li et al., 2013). The Tasna nappe is part of the northeastern European OCT preserving a wedge of continental crust that is laterally replaced by exhumed subcontinental mantle and grades into proto-oceanic crust with first magmatic additions (Manatschal et al., 2006). The Penninic Platta nappe is subdivided into two Alpine tectonic units, the Upper and the Lower Platta units (Supplementary material S1). The Upper Platta nappe is bounded at its top by the Lower Austroalpine Err nappe (part of the Adria distal continental margin) and overlies Middle and Lower Penninic nappes (remnant of the European distal margin; Manatschal and Nievergelt, 1997). Both the Platta and Tasna nappes, as well as the majority of Alpine-Apennine ophiolites, consist of highly serpentinized peridotites intruded by large gabbroic bodies and overlain locally by massive basaltic lava flows, continent-derived extensional allochthons and post-rift sediments (supplementary material S2, Desmurs, 2002; Desmurs et al., 2001; Peters et al., 2008).

2.2. Nature of the exhumed mantle

Two main types of mantle have been distinguished all around the Alpine-Tethys and more particularly in the Tasna and Platta nappes (Fig. 2a, Picazo et al., 2016). The first type identified in the Tasna and Upper Platta units consists of spinel lherzolites containing abundant garnet-bearing pyroxenites (Desmurs, 2002; Müntener et al., 2010; Peters et al., 2008). Major and trace element compositions in clinopyroxene demonstrate the fertile character of these mantle rocks (Picazo et al., 2016). This mantle, referred to as the inherited subcontinental mantle, is similar to the mantle exhumed in the proximal parts of the present-day Iberia-Newfoundland OCTs (Müntener and Manatschal, 2006).

70   The second type of mantle composing the lower Platta unit consists of spinel lherzolites with minor

71   harzburgites and dunites and shows only few occurrences of pyroxenites (Desmurs, 2002; Müntener et al.,

72   2010, 2004; Peters et al., 2008). This peridotite is pervasively impregnated by ascending tholeiitic melts

73   (Müntener et al., 2010, 2004) that pre-date the Middle Jurassic mantle exhumation (Piccardo, 2016; Rampone

74   et al., 1995). This mantle type has also been described from the distal part of the Iberia margin (Müntener and

75   Manatschal, 2006) and is considered to be the refertilized part of exhumed subcontinental mantle (see type 2

76   mantle in Picazo et al. 2016).

3. Basalts from the Platta and Tasna OCTs

3.1. Petrology of extrusive magmatic rocks and basaltic intrusions

79   Extrusive basaltic rocks exposed in the Platta and Tasna nappes (supplementary material S3) occur as

80   hyaloclastites, pillow breccias, pillow lavas and massive lava flows that can reach up to 300 m thickness (Fig.

81   2a-b). Basalts lie on exhumed mantle and are covered by Upper Jurassic to Lower Cretaceous marine sediments

82   (Fig. 2c). Basalts exhibit intersertal to porphyric textures and contain plagioclase phenocrysts embedded in a

83   fine-grained matrix of plagioclase, chlorite, epidote, pumpellyite and calcite (Fig. 2d). Hyaloclastite breccias

84   consist of fragments of lava flows, which probably derive from the dislocation of former volcanic deposits. A

85   Jurassic age (167-161 Ma) is based on the dating of radiolarian cherts that are either interlayered or overlie

86   the basalts (Bill et al., 2001) and U-Pb on gabbros that are genetically linked to the basalts (Schaltegger et al.,

87   2002).

88   A younger magmatic event consisting of sills of 10 to 20 m thickness (Fig. 2e) has been found in the Platta

89   nappe. These sills intrude limestones and shales of Lower Cretaceous age (Peters et al., 2008), representing

90   the youngest pre-Alpine magmatic event identified so far in the Alpine OCT. The sills are characterized by fine-

91   grained textures at the rims and coarse-grained at the center. They are composed of plagioclase, chlorite,

92   pumpellyite and epidote (Fig. 2f).

3.2. Major and trace element composition of basalts

A comprehensive description of analytical methods for chemical analysis are given in supplementary material S4. Major element content of our samples is similar to those of other basalts from the Platta nappe (Desmurs et al., 2002; Frisch et al., 1994). Considering both their mineralogical and geochemical compositions, they range between tholeiite and alkali basalt in nature (SiO_2: 45-50 wt.%; Al_2O_3: 15-19 wt.%; $Na_2O+K_2O < 5$ wt.%) and display relatively low Mg# (< 0.65) showing that they represent differentiated melts rather than primitive liquids (Table 1).

On the basis of trace element compositions, two different types of Jurassic basalts can be distinguished (Fig. 3). Type-1 is depleted in incompatible elements, shows a positive Zr anomaly, a low $(La/Sm)_N$ and is comparable to "normal" MORB. Type-1 shows a large fractionation of HREE over MREE, $(Sm/Yb)_N$=0.82-1.76, and a widespread Nb/La ratio (0.55 to 3.25). Samples characterized by medium to high HREE over MREE and a low Nb/La ratio are volumetrically predominant in the Platta-Tasna nappes as well as in the entire Alpine Tethys margins (Fig. 5). The type-2 is enriched in incompatible elements (>10 times PUM concentrations) and high field strength elements (HFSE, Nb, Ta, Zr, Hf; Fig. 3). Type-2 basalts have high $(La/Sm)_N > 1.3$ and high $(Sm/Yb)_N$>1.5 ratios, and are similar to present-day enriched MORB (E-MORB; Gale et al., 2013). Although of a different apparent age, trace element patterns of Cretaceous sills (type-3) are similar to those of Jurassic E-MORB. This geochemical diversity is not restricted to Platta and Tasna basalts but have been described in several ophiolites of the Alpine-Tethys domain (e.g. Bill et al., 2000 and Supplementary material S6).

4. Origin of OCT-basalts

Basalts from this study are representative of basalts from the Alpine-Tethys (Fig. 4). The Cr vs. Y diagram shows that all these basalts result from 5% to 15% partial melting followed by various degrees of fractional crystallization (Fig. 4). However, their variable trace element patterns (Fig. 3), illustrate that the Platta-Tasna basalts (types-1, 2 and 3) as well as other basalts from the Alpine Tethys may not derived from the melting of a depleted mantle source but rather may reflect the melting of another mantle source.

4.1. The depleted "N-MORB"-like basalts (type-1)

117

118   Type-1 basalts depletion in LREE makes them to a first order comparable to N-MORB (**Erreur ! Source**

119 **du renvoi introuvable.**a). However, most of these basalts as well as most of the Alpine-Tethys basalts

120 substantially differ from present-day MORB by lower Nb/La ratios and higher $(Sm/Yb)_N$ ratios (**Erreur ! Source**

121 **du renvoi introuvable.** and supplementary material S5). High $(Sm/Yb)_N$ ratios are classically used as a proxy to

122 identify the presence of a garnet-bearing component in the MORB source (Hellebrand et al., 2002; Montanini

123 et al., 2008; Saccani, 2015; Sobolev et al., 2007; Stracke et al., 1999). The melting of a DMM-like source in the

124 spinel stability field hardly produces basalts with $(Sm/Yb)_N > 1.2$, even at low degrees of melting, while most of

125 the Alpine basalts display $(Sm/Yb)_N > 1.2$ (see supplementary material S5). Such high $(Sm/Yb)_N$ ratios are easily

126 simulated by melting a depleted mantle source in the garnet stability. However, both modeling approaches

127 fail to reproduce the low Nb/La ratio that characterize most of the Alpine basalts (**Erreur ! Source du renvoi**

128 **introuvable.**b). Since Nb is more incompatible than La ($D_{Nb} < D_{La}$), Nb/La ratios tend to decrease in both the

129 residual mantle and the extracted melts with increasing melt degree. Thus, basalts with Nb/La<0.7 must be

130 derived from the melting of a mantle source more refractory than the asthenospheric DMM.

131   The inherited SCLM can hardly be considered as a potential source for type-1 basalts since it is too fertile

132 (mantle type 1a from Picazo et al., 2016) or too depleted (mantle type 1b from Picazo et al., 2016). Similarly,

133 the oceanic mantle (type 3 from Picazo et al., 2016) is too depleted and occurs too oceanward from the location

134 where basalts erupted. However, the refertilized mantle section (mantle type 2; Picazo et al., 2016) may be a

135 plausible source. The geochemical composition of this refertilized mantle is calculated following the modelling

136 approach of Müntener et al. (2010). The starting mantle composition is the PUM, which has undergone 4%

137 partial melting in the garnet (4%) stability field, followed by 4% in the spinel stability field. This residual mantle

138 is then refertilized by ascending melts (up to 12% in volume) deriving from the melting of an asthenospheric

139 depleted source (DMM) in the spinel stability field. Fig. 5a, b shows that the melting of such a refertilized

140 source is able to produce melts similar to type-1 basalts with low Nb/La and high $(Sm/Yb)_N$. The calculated

141 melting degree of the refertilized mantle is rather low (<15%), which is consistent with previous estimates

142   made on Alpine basalts (Desmurs et al., 2002). This model is very similar to the one proposed previously by

143   Meyzen et al., (2003) to explain the peculiar REE signature of some MORB from the northern magma-poor

144   section of the ultraslow-spreading Southwest Indian Ridge. More importantly, this model is consistent with

145   geological observations made by previous studies (Müntener et al., 2010; Picazo et al. 2016).

4.2.   The formation of "E-MORB"-like basalts (types-2 and 3)

147   Aside from type-1 basalts, a few percent of extrusive basalts can be ascribed as enriched-basalts (E-

148   MORB, types-2 and 3). Additional occurrences of E-MORBs have been reported previously in other fossil OCT

149   in the Alps (External Ligurides and Corsica; Montanini et al., 2008; Renna et al., 2018; Saccani et al., 2008). The

150   enriched nature of these basalts was attributed to the simultaneous melting of the Jurassic ascending

151   asthenosphere (i.e. the DMM) and garnet-pyroxenites. This hypothesis was tested by applying a similar

152   modeling approach to that of Montanini et al., (2008): variable amounts of garnet-pyroxenite derived melts

153   were mixed with (i) aggregated melts of a depleted spinel peridotite source (red mixing lines in **Erreur ! Source**

154   **du renvoi introuvable.**c, d) and (ii) type-1 basalts extracted from the refertilized SCLM (blue mixing lines in

155   **Erreur ! Source du renvoi introuvable.**c, d). Three different partial melting degrees are considered for the

156   formation of depleted melts (F=0.05, 0.1 and 0.15), while a high partial melting degree of 0.25 is considered

157   for the pyroxenite melt (Montanini et al., 2008). Other modeling features (partition coefficients, pyroxenite

158   source composition, etc.) are given in **Erreur ! Source du renvoi introuvable.** caption. Results highlight that E-

159   MORB melts may derive from the mixing between 80-90% of depleted MORB and 10-20% partial melts of

160   garnet-pyroxenite, these results being in good agreement with previous calculations of Sobolev et al., (2007)

161   and Montanini et al., (2008).

4.3.   Geodynamic constraints and conclusions

163   Ophiolites from the Alpine-Tethys domain have provided strong evidence for processes of interaction

164   between inherited SCLM and the ascending asthenosphere (Bodinier et al., 1991; Montanini et al., 2008;

165   Müntener et al., 2004; Müntener and Piccardo, 2003; Piccardo et al., 2004b, 2007; Tribuzio, 2004), which is

166 different from basalts formed at steady state, mature MORs. Almost all extrusive basalts from the Alpine-

167 Tethys OCT overlie an exhumed, refertilized SCLM (Picazo et al., 2016). Only a few overlie the inherited SCLM

168 in Central Alps (Upper Platta, Malenco, Totalp, Picazo et al., 2016). We therefore suggest here that the specific

169 geochemistry of basalts from the Alpine-Tethys OCT is related to their emplacement over the exhumed,

170 refertilized SCLM. The upward melt infiltration coming from the partial melting of the DMM in the garnet

171 stability field creates the widespread refertilized SCLM (type 2 mantle of Picazo et al. 2016). This melting

172 episode is enhanced by a near-adiabatic decompression regime (McKenzie and Bickle, 1988) during the very

173 first stages of lithospheric thinning and asthenospheric uplift (Piccardo et al., 2004a, Fig. 5a). Melt percolation

174 occurred during lithospheric/crustal thinning and was controlled by tectonic processes and the thermal

175 structure of the extending lithosphere, both of which are not well constrained. Kaczmarek and Müntener

176 (2010) proposed, using the example of the Lanzo shear zone, that percolation occurred in the footwall of a

177 major extensional shear zone that acted as a permeability barrier. The thermal advection related to both

178 asthenospheric upwelling and melt percolation is likely able to increase the thermal gradient in order to reach

179 the solidus of the refertilized SCLM at shallower depths in the spinel stability field (Piccardo et al., 2004a,

180 2004b). Integrating this inherited history of the SCLM may explain the peculiar geochemical signature

181 characterizing most of basalts from the Alpine-Tethys OCTs that were erupted on exhumed SCLM in the distal

182 part of the hyperextended margin (i.e. type-1 basalts, Fig. 5b). In contrast, the enriched basalts may correspond

183 to low degree melts of the DMM with small amounts of garnet-pyroxenite, both before and after the onset of

184 seafloor spreading (Fig. 5b-c). This study supports the idea that basalts erupting in the Alpine-Tethys OCT have

185 long-lived, poly-phase and variable mantle sources. The peculiar trace element geochemistry of basalts and

186 the well-established geodynamic setting of OCT in the Alps with complex mantle inheritance enable to explain

187 the differences between OCT and MOR basalts. Therefore, basalts formed along OCTs should be referred to as

188 OCT-basalts rather than MOR-basalts.

189

5. Acknowledgements

6. References

Anders, E., Grevesse, N., 1989. Abundances of the elements: Meteoritic and solar. *Geochim. Cosmochim. Acta,* **53**, 197–214. doi.org/10.1016/0016-7037(89)90286-X

Beccaluva, L., Ohnenstetter, D., Ohnenstetter, M., Venturelli, G., 1977. The trace element geochemistry of Corsican ophiolites. *Contrib. Mineral. Petrol.,* **64**, 11–31.

Beslier, M.-O., Royer, J.-Y., Girardeau, J., Hill, P.J., Boeuf, E., Buchanan, C., Chatin, F., Jacovetti, G., Moreau, A., Munschy, M., 2004. Une large transition continent-océan en pied de marge sud-ouest australienne: premiers résultats de la campagne MARGAU/MD110. *Bull. Soc. Geol. Française,* **175**, 629–641.

Bill, M., Nägler, T.F., Masson, H., 2000. Major, minor, trace element, Sm-Nd and Sr isotope compositions of mafic rocks from the earliest oceanic crust of the Alpine Tethys. *Schweizerische Mineralogische und Petrographische Mitteilungen*, **80-2**, 131-145.

Bill, M., O'Dogherty, L., Guex, J., Baumgartner, P.O., Masson, H., 2001. Radiolarite ages in Alpine-Mediterranean ophiolites: Constraints on the oceanic spreading and the Tethys-Atlantic connection. *Geol. Soc. Am. Bull.*, **113**, 129–143.

211   Bodinier, J., Guiraud, M., Dupuy, C., Dostal, J., 1986. Geochemistry of basic dikes in the Lanzo massif

212   (Western Alps): petrogenetic and geodynamic implications. *Tectonophysics*, **128**, 77–95.

213   Bodinier, J.-L., Menzies, M.A., Thirlwall, M.F., 1991. Continental to oceanic mantle transition—REE and Sr-Nd

214   isotopic geochemistry of the Lanzo lherzolite massif. *J. Petrol*., **2**, 191–210.

215   Chalot-Prat, F., Ganne, J., Lombard, A., 2003. No significant element transfer from the oceanic plate to the

216   mantle wedge during subduction and exhumation of the Tethys lithosphere (Western Alps). *Lithos*, **69**, 69–

217   103.

218   Chatin, F., Robert, U., Montigny, R., Whitechurch, H., 1998. La zone Diamantine (océan Indien oriental),

219   témoin de la séparation entre l'Australie et l'Antarctique: arguments pétrologiques et géochimiques.

220   Comptes Rendus Académie des Sciences, *Earth Planet. Sci.,* **326**, 839–845.

221   Chauvel, C., Bureau, S., Poggi, C., 2011. Comprehensive Chemical and Isotopic Analyses of Basalt and

222   Sediment Reference Materials. *Geostand. Geoanalytical Res*., **35**, 125–143. doi.org/10.1111/j.1751-

223   908X.2010.00086.x.

224   Chazot, G., Charpentier, S., Kornprobst, J., Vannucci, R., Luais, B., 2005. Lithospheric Mantle Evolution during

225   Continental Break-Up: The West Iberia Non-Volcanic Passive Margin. *J. Petrol.,* **46**, 2527–2568.

226   doi.org/10.1093/petrology/egi064.

227   Cornen, G., Girardeau, J., Monnier, C., 1999. Basalts, underplated gabbros and pyroxenites record the rifting

228   process of the West Iberian margin. *Mineral. Petrol.,* **67**, 111–142.

229   Desmurs, L., 2002. Mantle evolution and magmatism in an evolving ocean-continent transition: The Platta

230   nappe, eastern Switzerland. Diss., Naturwissenschaften, *ETH Zürich*, **14429, 2002**.

231   Desmurs, L., Manatschal, G., Bernoulli, D., 2001. The Steinmann trinity revisited: mantle exhumation and

232   magmatism along an ocean-continent transition: the Platta nappe, eastern Switzerland. *Geol. Soc. Lond.*

233   *Spec. Publ.,* **187**, 235–266.

234   Desmurs, L., Müntener, O., Manatschal, G., 2002. Onset of magmatic accretion within a magma-poor rifted

235   margin: a case study from the Platta ocean-continent transition, eastern Switzerland. Contrib. Mineral.

236   Petrol., **144**, 365–382. doi.org/10.1007/s00410-002-0403-4

237   Durand-Delga, M., Peybernès, B., Rossi, P., 1997. Arguments en faveur de la position, au Jurassique, des

238   ophiolites de Balagne (Haute-Corse, France) au voisinage de la marge continentale europeenne. *Académie*

239   *Sci.,* **325**, 973–981.

240   Dürr, S., Ring, U., Frisch, W., 1993. Geochemistry and geodynamic significance of North Penninic ophiolites

241   from the Central Alps. Schweiz. *Mineral. Petrogr. Mitteilungen,* **73**, 407–419.

242   Ferrara, G., Innocenti, F., Ricci, C.A., Serri, G., 1976. Ocean-floor affinity of basalts from north Apennine

243   ophiolites: geochemical evidence. *Chem. Geol.,* **17**, 101–111.

244   Frisch, W., Ring, U., Dürr, S., Borchert, S., Biehler, D., 1994. The Arosa Zone and Platta Nappe ophiolites

245   (Eastern Swiss Alps): geochemical characteristics and their meaning for the evolution of the Penninic Ocean.

246   *Jahrb Beol BA*, **137**, 19–23.

247   Gale, A., Dalton, C.A., Langmuir, C.H., Su, Y., Schilling, J.-G., 2013. The mean composition of ocean ridge

248   basalts: MEAN MORB. *Geochem. Geophys. Geosystems,* **14**, 489–518. doi.org/10.1029/2012GC004334

249   Hart, S.R., Dunn, T., 1993. Experimental cpx/melt partitioning of 24 trace elements. *Contrib. Mineral. Petrol.,*

250   **113**, 1–8.

251   Hellebrand, E., Snow, J.E., Hoppe, P., Hofmann, A.W., 2002. Garnet-field melting and late-stage refertilization

252   in 'residual' abyssal peridotites from the Central Indian Ridge. *J. Petrol.,* **43**, 2305–2338.

253   Herzberg, C., 2006. Petrology and thermal structure of the Hawaiian plume from Mauna Kea volcano. *Nature*,

254   **444**, 605.

255   Hirschmann, M.M., Stolper, E.M., 1996. A possible role for garnet pyroxenite in the origin of the "garnet

256   signature" in MORB. *Contrib. Mineral. Petrol.*, **124**, 185–208.

257   Ionov, D.A., Bodinier, J., Mukasa, S.B., Zanetti, A., 2002. Mechanisms and sources of mantle metasomatism:

258   major and trace element compositions of peridotite xenoliths from Spitsbergen in the context of numerical

259   modelling. *J. Petrol.,* **43**, 2219–2259.

260   Jochum, K.P., Brueckner, S.M., Nohl, U., Stoll, B., Weis, U., 2008. Geostandards and Geoanalytical Research

261   bibliographic review 2007. *Geostand. Geoanalytical Res.,* **32**, 509–514.

262   Johnson, K., Dick, H.J., Shimizu, N., 1990. Melting in the oceanic upper mantle: an ion microprobe study of

263   diopsides in abyssal peridotites. *J. Geophys. Res. Solid Earth,* **95**, 2661–2678.

264   Johnson, K.T.M., 1998. Experimental determination of partition coefficients for rare earth and high-field-

265   strength elements between clinopyroxene, garnet, and basaltic melt at high pressures. *Contrib. Mineral.*

266   *Petrol.*, **133**, 60–68. doi:10.1007/s004100050437

267   Kogiso, T., Tatsumi, Y., Nakano, S., 1997. Trace element transport during dehydration processes in the

268   subducted oceanic crust: 1. Experiments and implications for the origin of ocean island basalts. *Earth Planet.*

269   *Sci. Lett.*, **148**, 193–205.

270   Kramer, J., Abart, R., Müntener, O., Schmid, S.M., Stern, W.B., 2003. Geochemistry of metabasalts from

271   ophiolitic and adjacent distal continental margin units: Evidence from the Monte Rosa region (Swiss and

272   Italian Alps). *Swiss Bull. Mineral. Petrol.,* **83**, 217–240.

273   Lewis, A.D., Smewing, J.D., 1980. The Montgenevre ophiolite (Hautes Alpes, France): Meta—morphism and

274   trace-element geochemistry of the volcanic sequence. *Chem. Geol.*, **28**, 291–306.

275   Li, X.-H., Faure, M., Lin, W., and Manatschal, G., 2013. New isotopic constraints on age and magma genesis of

276   an embryonic oceanic crust: The Chenaillet Ophiolite in the Western Alps. *Lithos*, **160-161**, 283-291,

277   doi.org/10.1016/j.lithos.2012.12.016

278   Liberi, F., Morten, L., Piluso, E., 2006. Geodynamic significance of ophiolites within the Calabrian Arc. *Isl. Arc,*

279   **15**, 26–43.

280 Manatschal, G., Engström, A., Desmurs, L., Schaltegger, U., Cosca, M., Müntener, O., Bernoulli, D., 2006.

281 What is the tectono-metamorphic evolution of continental break-up: The example of the Tasna Ocean–

282 Continent Transition. *J. Struct. Geol*., **28**, 1849–1869. doi.org/10.1016/j.jsg.2006.07.014

283 Manatschal, G., Müntener, O., 2009. A type sequence across an ancient magma-poor ocean–continent

284 transition: the example of the western Alpine Tethys ophiolites. *Tectonophysics*, **473**, 4–19.

285 doi.org/10.1016/j.tecto.2008.07.021

286 Manatschal, G., Nievergelt, P., 1997. A continent-ocean transition recorded in the Err and Platta nappes

287 (Eastern Switzerland). *Eclogae Geol. Helvetiae*, **90**, 3–28.

288 Marroni, M., Molli, G., Montanini, A., Tribuzio, R., 1998. The association of continental crust rocks with

289 ophiolites in the Northern Apennines (Italy): implications for the continent-ocean transition in the Western

290 Tethys. *Tectonophysics,* **292**, 43–66.

291 Marroni, M., Pandolfi, L., 2007. The architecture of an incipient oceanic basin: a tentative reconstruction of

292 the Jurassic Liguria-Piemonte basin along the Northern Apennines–Alpine Corsica transect. *Int. J. Earth Sci.*,

293 **96**, 1059–1078. doi.org/10.1007/s00531-006-0163-x

294 Mazzeo, F.C., De Vita, P., Aulinas, M., Arienzo, I., Cirillo, G., Iovine, R.S., Sparice, D., 2016. New constraints on

295 the origin of the ophiolitic rocks within sin-orogenic turbiditic sequences at Cilento region (southern Italy).

296 *Geol. Acta Int. Earth Sci. J.,* **14**(3), 299-314.

297 McDonough, W.F., Sun, S.-S., 1995. The composition of the Earth. *Chem. Geol.,* **120**, 223–253.

298 McKenzie, D., Bickle, M. J. 1988. The volume and composition of melt generated by extension of the

299 lithosphere. *J. Petrol.* **29**, 625–679.

300 Meyzen, C.M., Toplis, M.J., Humler, E., Ludden, J.N., Mével, C., 2003. A discontinuity in mantle composition

301 beneath the southwest Indian ridge. *Nature*, **421**, 731–733. doi.org/10.1038/nature01424

302   Montanini, A., Tribuzio, R., Thirlwall, M., 2012. Garnet clinopyroxenite layers from the mantle sequences of

303   the Northern Apennine ophiolites (Italy): Evidence for recycling of crustal material. *Earth Planet. Sci. Lett.*,

304   **351**, 171–181. doi.org/10.1016/j.epsl.2012.07.033

305   Montanini, A., Tribuzio, R., Vernia, L., 2008. Petrogenesis of basalts and gabbros from an ancient

306   continent?ocean transition (External Liguride ophiolites, Northern Italy). *Lithos*, **101**, 453–479.

307   doi.org/10.1016/j.lithos.2007.09.007

308   Mugnier, J.-L., Cannic, S., Lapierre, H., 2008. The tholeiites of the Valaisan domain (Versoyen, western Alps): a

309   Carboniferous magma emplaced in a small oceanic basin. *Bull. Société Géologique Fr.,* **179**, 357–368.

310   Müntener, O., Manatschal, G., 2006. High degrees of melt extraction recorded by spinel harzburgite of the

311   Newfoundland margin: The role of inheritance and consequences for the evolution of the southern North

312   Atlantic. *Earth Planet. Sci. Lett.,* **252**, 437–452. doi.org/10.1016/j.epsl.2006.10.009

313   Müntener, O., Manatschal, G., Desmurs, L., Pettke, T., 2010. Plagioclase Peridotites in Ocean-Continent

314   Transitions: Refertilized Mantle Domains Generated by Melt Stagnation in the Shallow Mantle Lithosphere. *J.*

315   *Petrol.,* **51**, 255–294. doi.org/10.1093/petrology/egp087

316   Müntener, O., Pettke, T., Desmurs, L., Meier, M., Schaltegger, U., 2004. Refertilization of mantle peridotite in

317   embryonic ocean basins: trace element and Nd isotopic evidence and implications for crust–mantle

318   relationships. *Earth Planet. Sci. Lett.,* **221**, 293–308. doi.org/10.1016/S0012-821X(04)00073-1

319   Müntener, O., Piccardo, G.B., 2003. Melt migration in ophiolitic peridotites: the message from Alpine-

320   Apennine peridotites and implications for embryonic ocean basins. *Spec. Publ. Geol. Soc. Lond.,* **218**, 69–90.

321   Ottonello, G., Ernst, W.G., Joron, J.L., 1984. Rare earth and 3d transition element geochemistry of peridotitic

322   rocks: I. Peridotites from the Western Alps. *J. Petrol.,* **25**, 343–372.

323 Padoa, E., Saccani, E., Durand-Delga, M., 2001. Structural and geochemical data on the Rio Magno Unit:

324 Evidence for a new 'Apenninic' ophiolitic unit in Alpine Corsica and its geodynamic implications. *Terra Nova*,

325 **13**, 135–142.

326 Peters, T., Dietrich, V.J., Office fédéral de la topographie, 2008. Geologischer Atlas der Schweiz Blätt 1256

327 Bivio.

328 Picazo, S., Müntener, O., Manatschal, G., Bauville, A., Karner, G., Johnson, C., 2016. Mapping the nature of

329 mantle domains in Western and Central Europe based on clinopyroxene and spinel chemistry: Evidence for

330 mantle modification during an extensional cycle. *Lithos*, **266–267**, 233–263.

331 doi.org/10.1016/j.lithos.2016.08.029

332 Piccardo, G.B., 2016. Evolution of the lithospheric mantle during passive rifting: Inferences from the Alpine–

333 Apennine orogenic peridotites. *Gondwana Res.,* **39**, 230–249. doi.org/10.1016/j.gr.2016.03.001

334 Piccardo, G.B., 2008. The Jurassic Ligurian Tethys, a fossil ultraslow spreading ocean: the mantle perspective.

335 *Geol. Soc. Lond. Spec. Publ.,* **293**, 11–34. doi.org/10.1144/SP293.2

336 Piccardo, G.B., Müntener, O., Zanetti, A., 2004a. Alpine–Apennine ophiolitic peridotites: new concepts on

337 their composition and evolution. *Ofioliti*, **29**, 63–74.

338 Piccardo, G.B., Müntener, O., Zanetti, A., Pettke, T., 2004b. Ophiolitic peridotites of the Alpine-Apennine

339 system: mantle processes and geodynamic relevance. *Int. Geol. Rev.,* **46**, 1119–1159.

340 Piccardo, G.B., Padovano, M., Guarnieri, L., 2014. The Ligurian Tethys: Mantle processes and geodynamics.

341 *Earth-Sci. Rev.,* **138**, 409–434. doi.org/10.1016/j.earscirev.2014.07.002

342 Piccardo, G.B., Zanetti, A., Müntener, O., 2007. Melt/peridotite interaction in the Southern Lanzo peridotite:

343 Field, textural and geochemical evidence. *Lithos*, **94**, 181–209. doi.org/10.1016/j.lithos.2006.07.002

344 Pognante, U., Rösli, U., Toscani, L., 1985. Petrology of ultramafic and mafic rocks from the Lanzo peridotite

345 body (Western Alps). *Lithos,* **18**, 201–214.

346   Rampone, E., Hofmann, A., Piccardo, G., Vannucci, R., Bottazzi, P., Ottolini, L., 1995. Petrology, mineral and

347   isotope geochemistry of the External Liguride peridotites (Northern Apennines, Italy). *J. Petrol.,* **36**, 81–105.

348   Rampone, E., Hofmann, A.W., 2012. A global overview of isotopic heterogeneities in the oceanic mantle.

349   *Lithos*, **148**, 247–261. doi.org/10.1016/j.lithos.2012.06.018

350   Rampone, E., Hofmann, A.W., Raczek, I., 1998. Isotopic contrasts within the Internal Liguride ophiolite (N.

351   Italy): the lack of a genetic mantle–crust link. *Earth Planet. Sci. Lett.,* **163**, 175–189.

352   Rampone, E., Piccardo, G.B., Hofmann, A.W., 2008. Multi-stage melt–rock interaction in the Mt. Maggiore

353   (Corsica, France) ophiolitic peridotites: microstructural and geochemical evidence. *Contrib. Mineral. Petrol.,*

354   **156**, 453–475.

355   Renna, M.R., Tribuzio, R., Sanfilippo, A., Thirlwall, M., 2018. Role of melting process and melt–rock reaction

356   in the formation of Jurassic MORB-type basalts (Alpine ophiolites). *Contrib. Mineral. Petrol.,* **173**, 31.

357   Robertson, A., 2007. Evidence of continental breakup from the Newfoundland rifted margin (Ocean Drilling

358   Program Leg 210): Lower Cretaceous seafloor formed by exhumation of subcontinental mantle lithosphere,

359   and the transition to seafloor spreading. Presented at the Proceedings of the Ocean Drilling Program,

360   Scientific Results, pp 1–69.

361   Rudnick, R.L., Barth, M., Horn, I., McDonough, W.F., 2000. Rutile-Bearing Refractory Eclogites: Missing Link

362   Between Continents and Depleted Mantle. *Science*, **287**, 278–281. doi.org/10.1126/science.287.5451.278

363   Saccani, E., 2015. Continental Margin Ophiolites of Neotethys: Remnants of Ancient Ocean–Continent

364   Transition Zone (OCTZ) Lithosphere and Their Geochemistry, Mantle Sources and Melt Evolution Patterns.

365   *Episodes,* **38**. doi.org/10.18814/epiiugs/2015/v38i4/82418

366   Saccani, E., Principi, G., Garfagnoli, F., Menna, F., 2008. Corsica ophiolites: geochemistry and petrogenesis of

367   basaltic and metabasaltic rocks. *Ofioliti*, **33**, 207.

368   Schaltegger, U., Desmurs, L., Manatschal, G., Müntener, O., Meier, M., Frank, M., Bernoulli, D., 2002. The

369   transition from rifting to sea-floor spreading within a magma-poor rifted margin: field and isotopic

370   constraints. *Terra Nova*, **14**, 156–162.

371   Sobolev, A.V., Hofmann, A.W., Kuzmin, D.V., Yaxley, G.M., Arndt, N.T., Chung, S.-L., Danyushevsky, L.V.,

372   Elliott, T., Frey, F.A., Garcia, M.O., others, 2007. The amount of recycled crust in sources of mantle-derived

373   melts. *Science*, **316**, 412–417.

374   Steinmann, M., Stille, P., 1999. Geochemical evidence for the nature of the crust beneath the eastern North

375   Penninic basin of the Mesozoic Tethys ocean. *Geol. Rundsch.,* **87**, 633–643. doi.org/10.1007/s005310050236

376   Stracke, A., Salters, V.J., Sims, K.W., 1999. Assessing the presence of garnet-pyroxenite in the mantle sources

377   of basalts through combined hafnium-neodymium-thorium isotope systematics. *Geochem. Geophys.*

378   *Geosystems*, **1**, 12

379   Sun, Z., Stock, J., Jian, Z., McIntosh, K., Alvarez-Zarikian, C., Klaus, A., 2016. Expedition 367/368 scientific

380   prospectus: South China Sea rifted margin. *Int. Ocean Discov. Program*.

381   Tribuzio, R., 2004. Origin of the Gabbro-Peridotite Association from the Northern Apennine Ophiolites (Italy).

382   *J. Petrol.,* **45**, 1109–1124. doi.org/10.1093/petrology/egh006

383   Vannucci, R., Rampone, E., Piccardo, G.B., Ottolini, L., Bottazzi, P., 1993. Ophiolitic magmatism in the Ligurian

384   Tethys: an ion microprobe study of basaltic clinopyroxenes. *Contrib. Mineral. Petrol.,* **115**, 123–137.

385   Venturelli, G., Capedri, S., Thorpe, R., Potts, P., 1979. Rare-earth and other element distribution in some

386   ophiolitic metabasalts of Corsica, Western Mediterranean. *Chem. Geol.,* **24**, 339–353.

387   Venturelli, G., Thorpe, R.S., Potts, P.J., 1981. Rare earth and trace element characteristics of ophiolitic

388   metabasalts from the Alpine-Apennine belt. *Earth Planet. Sci. Lett.,* **53**, 109–123.

389   Workman, R.K., Hart, S.R., 2005. Major and trace element composition of the depleted MORB mantle

390   (DMM). *Earth Planet. Sci. Lett.,* **231**, 53–72.

391

7. List of figures and tables

393

394   Fig. 1: (a) Location of major ophiolite massifs in the Alps-Apennine-Corsica (redrawn after Rampone and

395   Hofmann, (2012); Schaltegger et al., (2002). [1]: Tertiary basins; [2]: European Units; [3]: Penninic Units; [4]:

396   Ophiolitic Units; [5]: Adriatic Units. (b) Schematic paleogeographic reconstruction of the Alpine-Tethys during

397   the Late Jurassic (redrawn after Picazo et al., 2016). The reconstruction is based on structural (Manatschal and

398   Müntener, 2009) as well as mantle geochemical (Picazo et al., 2016; Rampone and Hofmann, 2012)

399   considerations. Ophiolite with (*) highlight ambiguous paleo-location. CE: Cecina Valley, CH: Chenaillet, EL:

400   External Ligurides, ET: Erro-Tobbio, GE: Gets Nappe, IL: Internal Ligurides, LA: Lanzo, LP: Lower Platta, MA:

401   Malenco, MM: Monte Maggiore, MV: Mont-Viso, UP: Upper Platta, TA: Tasna, TO: Totalp, ZS: Zermatt-Saas.

402   Br: Briançonnais, Sa: Sardinia.

403

404   Fig. 2: Macroscopic field and microscopic observations of basalts. (a) Panoramic view of the Err-Platta Ocean-

405   Continent Transition zone illustrating the position of the inherited and refertilized (infiltrated) subcontinental

406   mantle. UP: Upper Platta; LP: Lower Platta; SCLM: subcontinental lithospheric mantle. (b) Platta outcrop with

407   gabbro body and refertilized mantle, overlain by basalt flows and radiolarian chert. Note that the topographic

408   surface is controlled by both Alpine thrusts and detachment faults. (c) Radiolarian chert sealing a basalt flow

409   (inverse serie). (d) Photomicrograph of Jurassic extrusive basalt showing plagioclase intersertal texture with

410   occurrence of little epidote. (e) Early Cretaceous basaltic sill intruding post-rift sediments. (f) Photomicrograph

411   of Cretaceous basaltic sill showing subhedral granular albitite (doleritic texture). Ep: epidote, Pl: plagioclase.

412

413   Table 1: Major and trace element compositions of basaltic rocks from the Tasna and Platta nappes. Mg# =

414   Mg/(Mg+Fe) (calculated in molar proportions).

415

Fig. 3: Whole-rock incompatible trace element (normalized to the primitive mantle, PM, McDonough and Sun, 1995) and rare-earth element compositions (normalized to C1 chondrite, Anders and Grevesse, 1989) of basalts from the Platta-Tasna nappes. (a) Type-1 depleted Jurassic extrusive basalts, (b) Type-2 enriched Jurassic extrusive basalts, (c) Type-3 Cretaceous basaltic sills. Dashed black lines N-MORB and E-MORB are from Gale et al., (2013) and other basalts from Platta are from Desmurs et al., (2002).

421

Fig. 4: Cr (ppm) versus Y (ppm) of whole-rock Platta-Tasna basalts. The partial melting trend starts from the mean DMM (Workman and Hart, 2005). The arrows indicate the calculated trends of the liquids for fractional crystallization of clinopyroxene + plagioclase (cpx + plg) assemblages starting from the relatively primitive basaltic sample 13-04 (residual liquid fraction F up to 0.5). Mineral mass fractions are 0.2cpx+0.8plg. Partition coefficients sources for Y and Cr are from Ionov et al., (2002) and from Hart and Dunn, (1993) respectively. Note that the starting mantle composition does not dramatically change the partial melting models nor the crystal fractionation trends. 1 : Gale et al., 2013, 2 : Other Platta basalts are from Desmurs et al., (2002) and Frisch et al., (1994). Alpine-Apennine basalts (little blue circles) are the overall Alpine-Tethys domain. Internal Ligurides (Ferrara et al., 1976; Ottonello et al., 1984; Rampone et al., 1998; Venturelli et al., 1981), External Ligurides (Marroni et al., 1998; Montanini et al., 2008; Vannucci et al., 1993; Venturelli et al., 1981), Corsica (Beccaluva et al., 1977; Durand-Delga et al., 1997; Padoa et al., 2001; Renna et al., 2018; Saccani et al., 2008; Venturelli et al., 1981, 1979), Western Alps (Bodinier et al., 1986; Chalot-Prat et al., 2003; Lewis and Smewing, 1980; Pognante et al., 1985), Central Alps (Desmurs et al., 2002; Frisch et al., 1994), Tuscany (Ferrara et al., 1976; Mazzeo et al., 2016), Calabre (Liberi et al., 2006) and inferred Valais domain (Bill et al., 2000; Dürr et al., 1993; Kramer et al., 2003; Mugnier et al., 2008; Steinmann and Stille, 1999).

437

438   Fig. 5: (a) Nb/La vs. La showing the compositions of Alpine basalts. The modelling consists of the calculation of

439   Nb/La ratio of aggregated non-modal fractional liquids that derive from the partial melting of the refertilized

440   SCLM. The chemistry of the refertilized mantle source is calculated following the study of Müntener et al.

441   (2010) : a fertile peridotite (primitive upper mantle, PUM; McDonough and Sun, 1995) experienced 4% partial

442   melting in the garnet stability field (A) followed by 4% of additional melting in the spinel stability field (B). The

443   residue is refertilized by adding a 4% fractional melt derived from a spinel DMM source (1% increment, C). A

444   volume of 1%, 3%, 6%, 9% and a maximum of 12% of melts stored in the peridotite is considered (Müntener

445   et al., 2010). The red curves correspond to melts extracted from the calculated refertilized mantle in the spinel

446   stability field at F up to 20%. Partition coefficients are from Johnson et al., (1998), starting mineralogy and

447   modes are from Johnson et al., (1990). (b) $(Sm/Yb)N$ vs. Yb_N of alpine basalts. Red curves are calculated in the

448   same way as in Fig. 5a. (c) Nb/La vs. La of E-MORB alpine basalts, assuming that they derive from the mixing of

449   aggregated non-modal fractional melts (F=5, 10, 15%) from a spinel DMM source (in red) or a refertilized SCLM

450   (8% refertilization, in blue) with garnet pyroxenite derived melts (F=25%; Montanini et al., 2008). The garnet

451   pyroxenite source derives from high degrees of batch melting (F=40%; Montanini et al., 2012) of a recycled

452   oceanic crust (i.e. an eclogite; Sobolev et al., 2007). The eclogite composition ($C_{eclogite}$) is calculated assuming

453   that eclogite corresponds to basaltic, N-MORB type crust (C_{N-MORB}) that experienced element mobility during

454   subduction prior being recycled into the mantle: $C_{eclogite}= C_{N-MORB}$ - retention factors where retention factors =

455   1 - mobility coefficients (Kogiso et al., 1997). The calculated eclogite has a high Nb/La ratio (~2, not shown

456   here), consistent with values calculated by Rudnick et al., (2000). Gt-pyroxenite mineralogy: 60% cpx, 30% opx,

457   10% gt (Hirschmann and Stolper, 1996); melting modes: cpx=gt=50%. Eclogite mineralogy: 50% gt, 50% cpx.

458   Numbers in italic represent the proportion of mantle derived melts in the mixing. (d) $(Sm/Yb)_N$ vs. Yb_N of alpine

459   basalts. Red and blue curves are calculated in the same way as in Fig. 5c. N-star: N-MORB average ± 2σ (grey

460   area); Present-day MORBs and N-MORB average are from Gale et al. (2013).

461

462   Fig. 5 : Schematic representation of the geodynamic model leading to the OCT-basalts. (a) Melt percolation.

463   Near adiabatic upwelling of the asthenosphere (DMM) during this early rifting stage. Onset of asthenosphere

464   partial melting in the garnet stability field (pink circles), and initial percolation of melts towards the

465   subcontinental mantle (light brown area) during the stretching of the lithosphere. Porous-flow melt

466   percolation induces (i) the refertilization of Permian (?) depleted SCLM, (ii) the formation of plagioclase-

467   bearing peridotite at shallower levels, and (iii) the formation of a weakened mantle wedge for the lithospheric

468   breakup (Piccardo, 2016). The distal subcontinental mantle is melt-impregnated (up to 12%) and refertilized.

469   Major crustal/lithospheric thinning is followed by mantle exhumation and onset of sea-floor exposure of the

470   melt-modified peridotites. (b) Creation of OCT-basalts. Thermal advection (Piccardo et al., 2014) enhanced by

471   porous-flow melt percolation moves the solidus upwards allowing the melting of the refertilized

472   subcontinental mantle in the spinel stability field (light blue circles) forming the type-1 basalts (light blue pipes

473   and volcanoes). Mixing of melts from the partial melting of the DMM (dark blue circles) and garnet-pyroxenite

474   (black dashes, orange circles) creates type-2 basalts (red pipes and volcanoes). (c) Formation of type-3 off-axis

475   basalts (yellow volcanoes) by the same process as type-2. The mixing between the two sources is located at

476   the two edges of the upwelling asthenosphere and is probably related to thermal readjustments. Active

477   spreading ridge followed by MOR-basalt formation caused by the partial melting of the DMM under spinel

478   (shallow) stability field.

479

8. Supplementary material

481

482   Supplementary material S1: (a) Location of the Platta and the Tasna nappes in the Alpine realm. (b) Tectonic

483   units and paleogeographic domains close to Platta and Tasna Nappes. (c) Geological map of Platta modified

484   after Schaltegger et al., (2002). with sample locations. Cretaceous magmatic sills (red) have been magnified

485   for clearance.

486   Supplementary material S2: Schematic section representing the lithologies and their stratigraphic position in

487   the Platta nappe. Note that the shear-zone in mantle and the sulfide deposit are truncated by the

488   detachment fault. Redrawn after Peters et al., (2008) and own fieldwork observations.

489   Supplementary material S3: Locations and mineralogical assemblage of studied magmatic samples.

490   Coordinates grid is WGS84 UTM 32N, decimal degrees. Fds (Ab): feldspar (albite), Cal: calcite, Chl: chlorite,

491   Cpx: clinopyroxene, Ep: epidote. Crosses indicate relative mineral proportions. Note that samples 13-03 and

492   13-04 are from the Tasna nappe.

493   Supplementary material S4: Analytical method
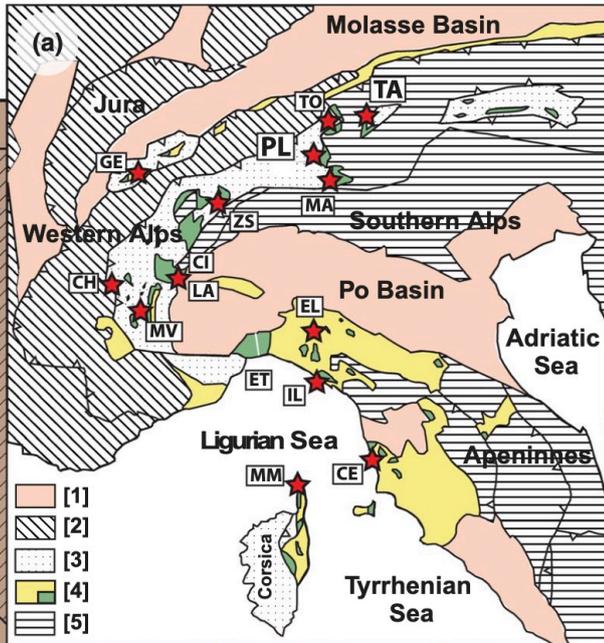
494   Major and trace elements were measured using the analytical method of Chauvel et al., (2011) at

495   Laboratoire d'Hydrologie et de Géochimie de Strasbourg (LHyGeS, University of Strasbourg, France). For major

496   elements, ~50 mg of sample powder was precisely weighted and dissolved in closed Savilex® beakers using a

497   mixture of 0.3 mL HF 24N and 0.85 mL HNO_3 14N in a hot plate at 90°C for 5 days. 20 ml of boric acid (H_3BO_3

498   at 20 g.l^{-1}) was added to the solutions after cooling to neutralize excess HF and were further diluted with 250

499   ml of Milli-Q® water. The solutions were then stored in a refrigerator for at least 2 days to ensure complete

500   neutralization of HF by H_3BO_3 and analyzed within a week using an ICP-AES (Thermo Scientific ICAP 6500). For

501   trace elements, 100 mg of sample powder were dissolved in a HF-$HClO_4$ mixture (5:1) in closed teflon beaker

502   on a hot plate at 140°C for 7 days. The mixture was then completely evaporated at 150°C, and the residue was

503   taken up in concentrated HNO_3. After another complete evaporation, the residue is finally diluted in 40 mL of

504   HNO_3 7N. The international standard PM-S (gabbro) was analysed repeatedly as unknown to ensure the validity

505   of our measurements. Results show that PM-S concentrations are consistent with the preferred reference

506   values from GeoREM (Jochum et al., 2008). Differences are less than 0.6% for SiO_2 and less than 2% for all

507   other major oxides except for Na_2O, K_2O and P_2O_5 which are present in very low concentrations. In addition,

508   sample 24-04 has been analyzed twice as a duplicate and results show no relevant differences in trace

509   elements between the two aliquots. It is noticed that the anomalous composition of one sample (20-03), which

510   is characterized by very low SiO_2 (36.92 wt.%), high CaO (15.33 wt.%) and high LOI (9.33 wt.%), is explained by

511   the amount of calcite veins and is not used in the discussion.

512

513   Supplementary material S5: (a) $(La/Sm)_N$ vs. $(Sm/Yb)_N$ of Alpine basalts compared to present-day MORBs (Gale

514   et al., 2013). Sample position reflects their shape of REE patterns, which depends on melting processes and/or

515   the source composition. Most of present-day MORBs (N-MORBs) are explained by moderate to high degrees

516   of partial melting (Gale et al., 2013) of a depleted mantle source in the spinel stability field (Workman and

517   Hart, 2005) as represented by the small graph in the lower left corner. In contrast, most Alpine basalts

518   (including basalts from the Platta and Tasna nappes) are characterized by high $(Sm/Yb)_N$, suggesting the

519   involvement of garnet in the mantle source. Samples that plot in the upper right part of the graph (i.e. E-MORB)

520   can be related to low degrees of melting of a garnet depleted mantle source although they more likely derive

521   from the melting of an heterogenous, enriched source. N-star: N-MORB average $\pm 2\sigma$ (grey area); E-star: E-

522   MORB average (Gale et al., 2013). PM: partial melting, sp: spinel, gt: garnet. (b) Nb/La vs. $(Sm/Yb)_N$ of Alpine

523   basalts compared to present-day MORBs. The calculated aggregated non-modal fractional melts derived from

524   a spinel lherzolite (in red) and a garnet lherzolite (in green) are shown. The mantle source chemistry is the

525   DMM from Workman and Hart, 2005, and results using the enriched (E-) and depleted (D-)DMM are also shown

526   to not have a narrow vision of the heterogeneous geochemistry of the DMM. Numbers in italic indicate the

527   degree of partial melting. Partition coefficients are from Johnson et al., (1998), starting mineralogy and modes

528   are from Johnson et al., (1990).
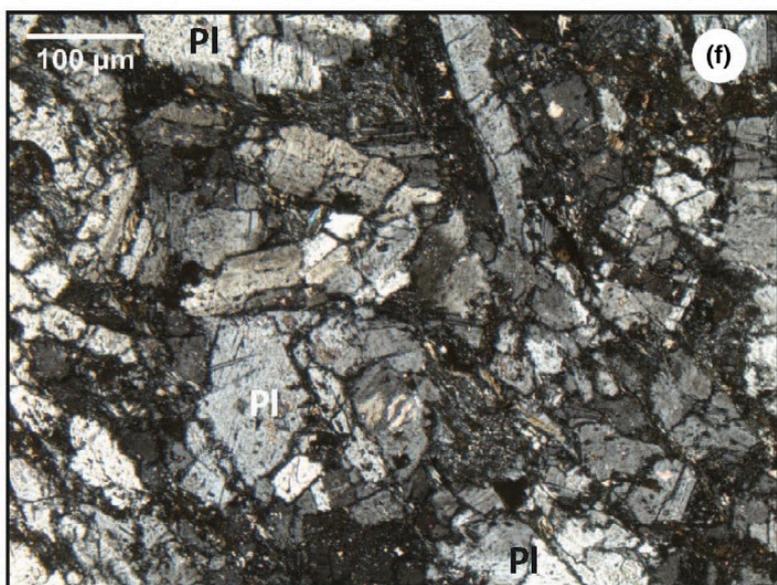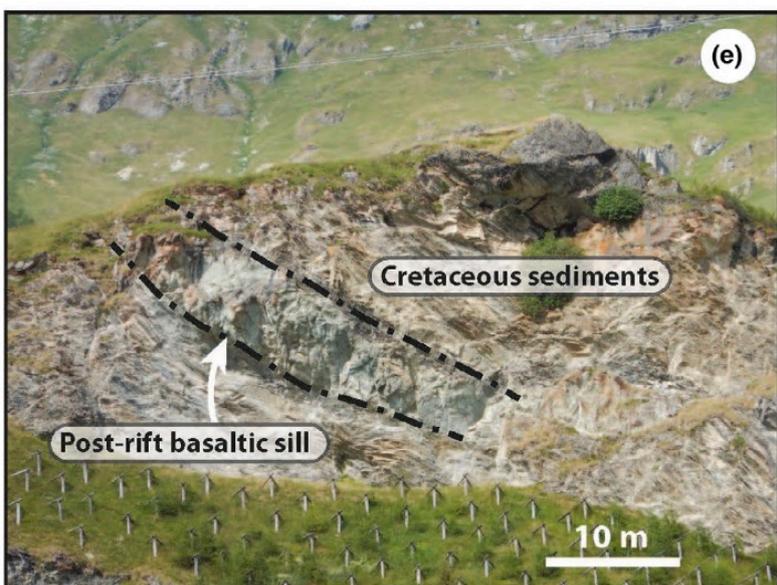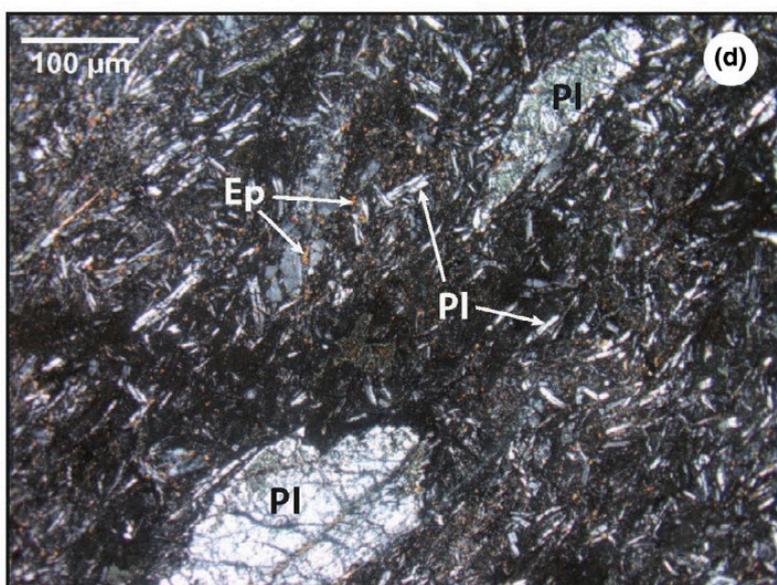
529

530

(a)

Molasse Basin

Jura

Western Alps

TO

TA

PL

GE

ZS

CI

MA

Southern Alps

CH

LA

Po Basin

EL

MV

ET

IL

Adriatic Sea

Ligurian Sea

Apeninnes

MM

CE

Corsica

Tyrrhenian Sea

[1]
[2]
[3]
[4]
[5]

(b)

Eastern Alps

Western and Central Alps sections

TA

ZS

Br

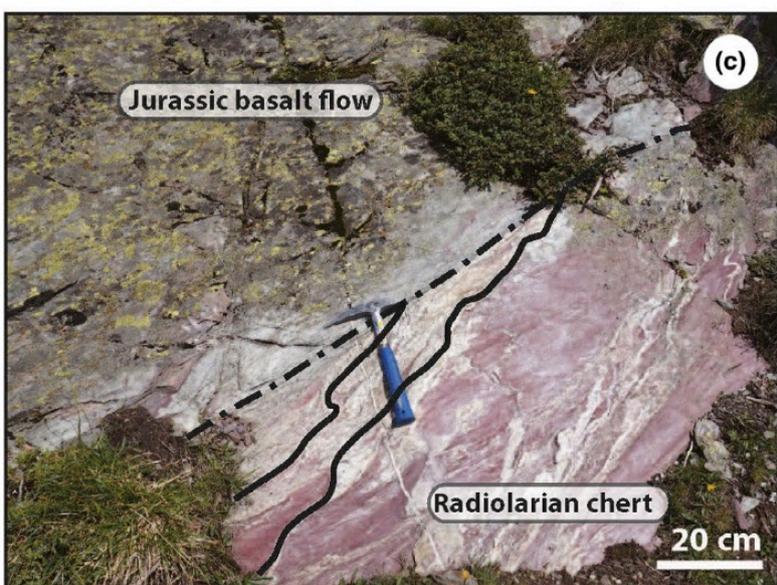GE

CH

MV

TO

LP

UP

Adria

MA

MM

Sa

Europe

Pyrenees

Paleo-Tethys Ocean

Iberia

LA*

ET

Apulia

EL

IL

CE*

Liguria-Piemonte Basin

Thinned/Undeformed continental crust

Inherited and/or depleted SCLM

Refertilized SCLM

Oceanic lithospheric mantle (DMM)

(a)

Falotta

W   E

← OCEANWARDS

Alpine thrusts

Detachment fault

Ophicalcite front

| Continental crust (Err Unit) |
| Basalts |
| Refertilized (lw. PL) |
| Inherited (up. PL) |

SCLM

(b)

WNW   *Pare Neira (2430)*   ESE

Radiolarian chert

Basalt flow

Ransung

Refertilized mantle

Basalt flow

Gabbro body

(c)

Jurassic basalt flow

Radiolarian chert

20 cm

(d)

100 µm

Pl

Ep

Pl

Pl

(e)

Cretaceous sediments

Post-rift basaltic sill

10 m

(f)

100 µm

Pl

Pl

Pl

(a) Type-1: depleted Jurassic extrusive basalts — N-MORB

(b) Type-2: enriched Jurassic extrusive basalts — E-MORB

(c) Type-3: Cretaceous basaltic sills — E-MORB

(a) Nb/La vs Nb diagram with PUM reference point and melting curves for refertilized SCLM.

(b) $(Sm/Yb)_N$ vs Yb_N diagram with PUM reference and melting trends.

Legend (panel a, b): **Melting of refertilized SCLM**
- 12% refertilization
- 9% refertilization
- 6% refertilization
- 3% refertilization
- 1% refertilization

(c) Nb/La vs Nb diagram with Gt pyroxenite melts.

(d) $(Sm/Yb)_N$ vs Yb_N diagram with Gt pyroxenite melts.

Legend (panel d): **Platta & Tasna basalts**
- Type 1
- Type 2
- Type 3
- Alpine basalts
- Present-day MORBs

Melting (F) of the mantle source
- 15%
- 10%
- 5%

(a) Melt percolation

0 km

brittle to ductile transition

30 km

60 km

1300°C

Adiabatic exhumation > Thermal erosion

(b) OCT-basalts

0 km

30 km

1300°C

60 km

Adiabatic exhumation < Thermal erosion

(c) MOR-basalts

Active spreading ridge

0 km

30 km

Adiabatic exhumation > Thermal erosion

1300°C

60 km

Continental crust

Permian underplatted gabbro

Inherited+garnet-pyroxenite layers
(subcontinental mantle)

Permian depletion

Refertilized mantle

Asthenosphere (DMM)

Active thermal erosion
Solidus

Active adiabatic exhumation
Boundary DMM/SCLM

Refertilization process

Porous melt flow percolation

Partial melting of DMM

OCT-basalt

Type 1 basalt

Type 1
Channelized melt flow
Partial melting of the refertilized
subcontinental mantle

Type 2 basalt

Type 2
Mixing melt flow
Partial melting of the DMM
and garnet-pyroxenite

Type 3 basalt

Type 3
Mixing melt flow
Partial melting of the DMM
and garnet-pyroxenite

MOR-basalt

MORB
Channelized melt flow
Partial melting of the DMM

(a)

Molasse Basin

Jura

PLATTA TASNA

Western Alps

Southern Alps

Po Basin

Adriatic Sea

Apennines

Tyrrhenian Sea

- Tertiary basins
- European Units
- Briançonnais/Valais
- Liguria Piemonte-ophiolites
- Adriatic Units

Chur
PRATTIGAU
TOTALP
AROSA
Davos
TASNA
13-03,04
SILVRETTA
Engadine line
SESVENNA
Ortler
CHAMS
ERR
St. Moritz
PLATTA
Bivio
CAMPO
SURETTA
AVERS
BERNINA
GRUF
MARGNA
BERGELL
MALENCO
Poschiavo
N
Insubric line
10km

Chur
9°40' 9°50' 10°00' 10°10'
46°50'
46°40'
46°30'
46°20'
46°10'

(b)

ALPINE TECTONIC UNIT	TETHYS PALEO-GEOGRAPHIC DOMAIN

PENNINIC NAPPE

South Pennine — Piemont-Liguria Ocean

Central Pennine (cover nappe) — Detached Mesozoic cover of the Briançonnais microcontinent

Central Pennine (basement nappe) — Variscan basement nappe affected by alpine HP metamorphism

North-Pennine — Valais Ocean

LOW. AUSTROALPINE NAPPE — Lower Austroalpine (basement nappes) — Adria distal continental margin

MARGNA NAPPE — Upper and lower crustal slices — Extensionnal allochthons in the transition between Adriatic margin and Alpine Tethys

CENT. AUSTROALPINE NAPPE — Upper Austroalpine and South Alpine nappes — Pre-Permian basement in general

EUROP. CONT. — Metamorphic nappes — Distal European margin

ADRIA CONT. — South Alpine — Undeformed Adria microplate

GRANITES — Bergell granite

(c)

P. Colm
46°34'
46°33'
24-01
14-02
21-05
21-02
20-03
46°32'
Mulegns
Sur
46°31'
Marmorera
46°30'
P. Platta
03-01
22-08
26-05
25-02
△P. Scalotta
46°29'
Bivio
24-04
46°28'
N
2 km
06-06
46°27'
9°36' 9°38' 9°40' 9°42'

exhumed mantle domain (Ocean-Continent-Tansition zone)

oceanwards ← → continentwards

distal margin

Lower Serpentinite Unit	Upper Serpentinite Unit	Err Unit (continental crust)
post-rift sediments		(not differentiated)
basalts		
gabbros		major alpine Cretaceous thrust contacts
serpentinized mantle		

Cretaceous sills

Turba normal fault

CRETACEOUS
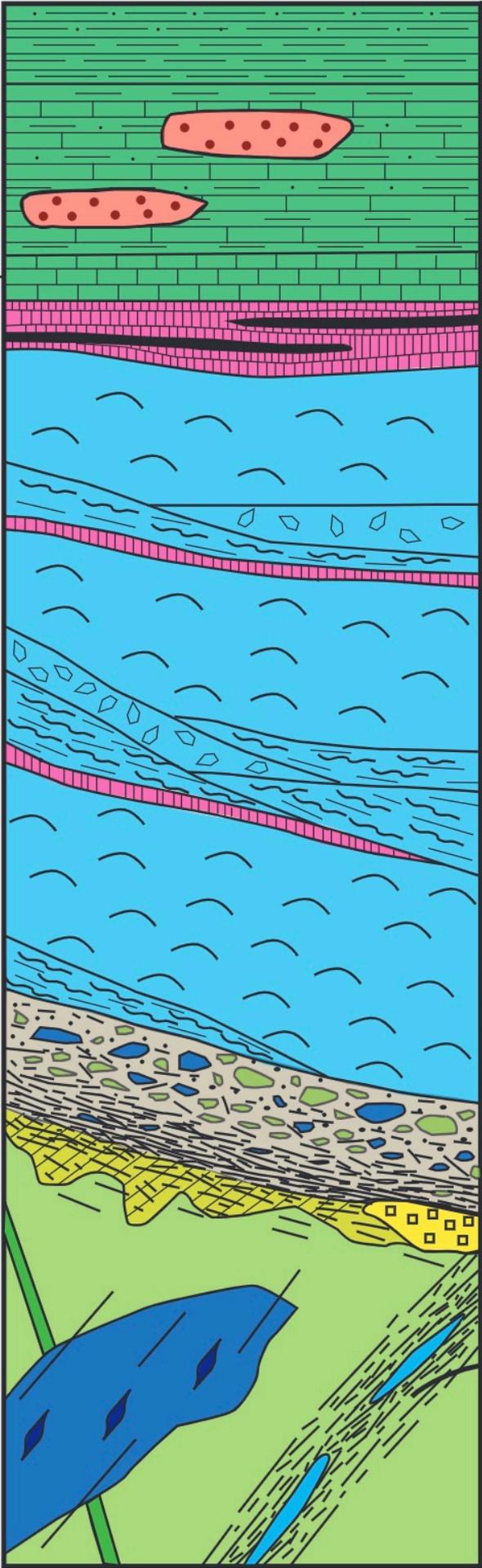
JURASSIC

Tonschiefer and Palombini

Aptychus limestone

Legend:

- phyllite, schist
- alkali-gabbro
- calc-schist and calcarenite
- limestone
- Mn-deposit
- hyaloclastite flow/pillow breccia
- radiolarian cherts
- basalt flow and pillow basalt
- sulfide deposit
- ophicalcite
- rodingite dike
- gabbro with sigmoidal magmatic pocket
- mantle-derived rocks and garnet-pyroxenite layers

Detachment fault
(gouge, breccia with gabbro and serp. clasts)

Shear-zone
(rodingitized basaltic dikes)